ACS Sustainable Chemistry & Engineering

pubs.acs.org/journal/ascecg

Research Article

Energy-Saving Effect of Low-Cost and Environmentally Friendly Sepiolite as an Efficient Catalyst Carrier for CO_2 Capture

Rui Zhang,* Yufan Li, Yiming Zhang, Ting Li, Luning Yang, Chao'en Li, Francesco Barzagli,* and Zhien Zhang*

Cite This: https://doi.org/10.1021/acssuschemeng.2c06739

Read Online

ACCESS | Metrics & More | Article Recommendations

ABSTRACT: Recently, the development of efficient solid acid catalysts to promote the CO_2 desorption rate while reducing energy consumption has attracted much attention. In this work, low-cost environmentally friendly sepiolite (SEP) clay was evaluated as a support of metal oxide (Fe_2O_3, CuO) catalysts. By comparing their catalytic performances for CO_2 desorption from CO_2-rich monoethanolamine (MEA) solution at 100 °C, the obtained results showed that the tested catalysts can accelerate the CO_2 release rate and reduce heat consumption in comparison with the non-catalytic MEA solution. The relative heat duty found decreased in the following order: blank (100%) > SEP (66.4%) > CuO-SEP (58.8%) > Fe_2O_3-SEP (54.0%). Recycling tests to study stability demonstrated that Fe_2O_3-SEP can maintain its catalytic efficiency after six recycling runs. Characterization studies revealed that a high mesoporous specific surface area and a high ratio of Brønsted and Lewis acid sites are beneficial to enhancing the activity of the catalysts. In addition, a possible catalytic mechanism for CO_2 desorption was proposed. As a result, this work proved that SEP has the potential to be a low-cost and competitive catalyst carrier for CO_2 capture.

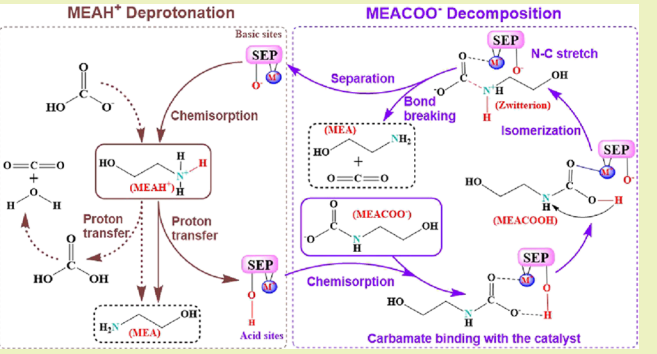

KEYWORDS: *carbon capture, monoethanolamine, heat consumption, catalysts, sepiolite, catalytic mechanism*

INTRODUCTION

Carbon dioxide (CO_2) has been accused as one of major responsible contributors for the increasingly serious climate problem due to the rising concentration of CO_2 in the atmosphere.[1] CO_2 capture technology has been investigated widely for controlling CO_2 emissions from industrial flue gas, and the amine-based chemical absorption process has been regarded as the most mature method for the post-combustion CO_2 capture.[1,2] However, the large-scale application of amine-based CO_2 capture technology is still challenging, mainly because of the huge heat requirement in the amine solvent regeneration process (CO_2 desorption).[3,4] Many efforts have been made to overcome the drawbacks of the amine-based CO_2 capture technology including the development of new absorbents and the use of other new technologies for enhancing the CO_2 capture efficiency.[5−11] It was reported that the heat cost for solvent regeneration contributes more than 70% of the total heat cost, which constrains the industrial application of this technology.[3,12]

The heat consumption in the solvent regeneration process consists of reaction heat, evaporation heat, and sensible heat.[12] To regenerate the amine solvent, the traditional method involves supplying heat to release CO_2 from the CO_2 species, namely, carbamate and bicarbonate/carbonate, by breaking the C−N and C−O bonds, respectively. On the other hand, it is also necessary to supply heat for endothermic deprotonation of the protonated amine. The heat requirement to restore the amine determines that the solvent regeneration (CO_2 desorption) process must be performed at a high desorption temperature, normally at 120−140 °C.[13] High temperature results in high energy consumption. Moreover, the high desorption temperature causes degradation of the absorbent and the CO_2 capture efficiency is expected to decrease after a long running period.

Recently, the solid acid catalyst-aided CO_2 desorption process has attracted much attention aiming to minimize the energy consumption of the process:[14−18] the addition of solid acid catalysts allows the CO_2 desorption process to be performed at a relatively low temperature (below 100 °C),

Received: November 10, 2022
Revised: February 17, 2023

which not only accelerates the CO_2 desorption rate but also decreases the heat consumption for releasing CO_2. It is commonly accepted that the main contributors for the high heat consumption during CO_2 desorption are the carbamate decomposition and deprotonation of protonated amine, and both processes involve proton transfer.[13,19] Solid acid catalysts can promote the two reaction processes mentioned above because of their remarkable acidity and the presence of the Brønsted and Lewis acid sites.[20] Liang et al.[21] reported that the solid catalyst HZSM-5 (Brønsted acid dominated) and γ-Al_2O_3 (Lewis acid dominated) can reduce the heat duty efficiently in the commercial aqueous monoethanolamine (MEA) solution regeneration process. Recently, Bhatti et al.[22] investigated several metal oxide catalysts to improve CO_2 desorption performance in nonaqueous 2-(2-aminoethoxy)ethanolamine (DGA) solution at the desorption temperature of 90 °C; as a result, WO_3 and TiO_2 showed remarkable advantages in enhancing the CO_2 desorption performance. Zhang et al.[23] studied SAPO-34 and SO_4^{2-}/TiO_2 for the catalytic CO_2 desorption from CO_2-loaded MEA solution under the relatively low temperature of 96 °C; their results revealed that the Brønsted/Lewis acid sites on the catalysts are beneficial to the $MEAH^+$ deprotonation and carbamate decomposition, and a high mesopore surface area (MSA) also enhances the catalytic CO_2 desorption performance. Zhang et al.[19] loaded several metal oxides, namely, CuO, Fe_2O_3, and NiO, over KIT-6 to prepare new catalysts for CO_2 desorption, and a remarkable decrease in the heat consumption (by 33.4%) was observed when CuO-KIT-6 was used, which confirmed that MSA is an important indicator for improving the catalytic performance. In addition, Xing et al.[24] selected SO_4^{2-}/ZrO_2 as an active component loaded on the HZSM-5 catalyst to improve the Brønsted/Lewis acid sites, and their results showed that the desorption rate was increased significantly with the aid of the SO_4^{2-}/ZrO_2-HZSM-5 catalyst in comparison with the non-catalytic process. Furthermore, the heat consumption in the solvent regeneration process decreased up to 30% as well.

However, with different catalyst carriers, the same catalyst, for example, SO_4^{2-}/ZrO_2, shows different catalytic performances.[24−28] Unfortunately, the current reported catalyst carriers were normally synthesized using complicated, cost-expensive, and environmentally unfriendly preparation methods, which prohibits the large-scale application of catalytic CO_2 desorption technology. Therefore, finding a stable, environmentally friendly carrier with a proper pore structure can be very helpful to promote the catalytic CO_2 desorption process.

Recently, natural clay materials have raised the interest of scientists because of their competitive porous properties, low cost, easy acquirement, and environment friendliness and they have been widely used for the preparation of adsorption materials and catalysts.[29−32] Tan et al.[13] investigated attapulgite (ATP) as a cost-effective catalyst to catalyze the CO_2 desorption, capable of increasing the CO_2 desorption rate by 54−57% while reducing the heat duty by 32%. Bhatti et al.[32] exploited different acids to activate the montmorillonite (Mont) and used them to catalyze CO_2 desorption. They found that all acid-activated Mont catalysts showed high catalytic activity, especially the H_3PO_4-activated Mont catalyst (PO_4-Mont), which was able to reduce the heat duty by 32.4% and increase the desorption rate by 75%. Moreover, they modified Mont via ion exchange using H_2SO_4 and Zr was able to improve the CO_2 desorption rate by up to 215% and reduce the heat duty by up to 44.15%.[31] Bhatti et al.[33] further used Fe and Co to enhance the catalytic activity of Mont, achieving a 315% increase in CO_2 desorption and a 40% decrease in heat duty. In addition, the work of Tan et al.[34] further indicates that the metal oxides can enhance the catalytic CO_2 desorption performance of ATP in terms of the amount of desorbed CO_2 and heat duty. It is noteworthy that all studied clay-based catalysts demonstrated prominent stability after the recycling experiments in the laboratory test.

Sepiolite (SEP, $Si_{12}O_{30}Mg_8(OH)_4(H_2O)_4{\cdot}8H_2O$) as one of the clay minerals has the same layered structure with Mont; however, it has insufficient octahedral sheets in comparison with the latter.[35] SEP is a pure trioctahedral mineral in the form of two-dimensional tetrahedral sheet of SiO_5.[36−38] The platelet edges on the SEP structure normally have a few positive charges that can stretch the species with negative charges. Meanwhile, the −OH and anionic groups on the SEP surface can participate in chemical reactions and extend the crystal interlayer spacing.[38] Figure 1 shows the schematic structure of SEP: due to the presence of the cations and the three kinds of water in the structure, SEP can have both Brønsted and Lewis acid sites available when it reacts with other species. These peculiarities might have potential to promote the CO_2 desorption process. Furthermore, more works have proved that the metal oxides can further improve the CO_2 desorption performance of the catalyst carrier.[13,39,40] In addition, when the surface of the metal oxide is exposed to water, more acidic Brønsted (−OH) sites can be generated, which promote the $MEACOO^-$ decomposition.[39] Hence, since SEP is a natural clay mineral and an easy material to obtain, it is worth to be investigated when it is used as a catalyst carrier to combine with metal oxides in the CO_2 desorption process in terms of the CO_2 desorption rate, the amount of desorbed CO_2, and the heat consumption.

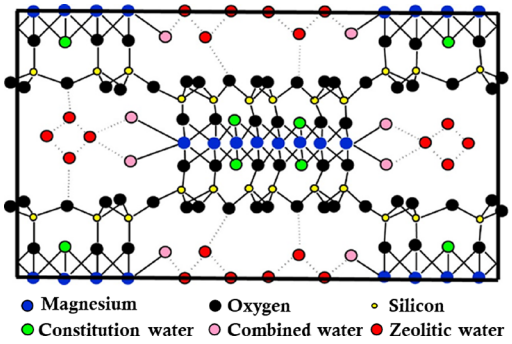

Figure 1. Schematic structure of sepiolite (SEP).

EXPERIMENTAL SECTION

Chemicals. High- or ultra-high-purity gases used in this work including CO_2 (99.999%) and nitrogen (N_2, 99.9%) were acquired from Hunan Zhongtai Hongyuan Gas Co., Ltd. The materials used for the catalyst preparation including iron(III) nitrate nonahydrate ($Fe(NO_3)_3{\cdot}9H_2O$, 98.5%), copper nitrate trihydrate ($Cu(NO_3)_2{\cdot}3H_2O$, 99%), and MEA (99%) were purchased from Shanghai Macleans Biochemical Co., Ltd., while SEP was acquired from Hunan Lihengtong New Material Co., Ltd. All chemicals were used without further purification in this work.

Catalyst Preparation. The impregnation method was used to prepare the catalysts in this work. A certain amount of $Fe(NO_3)_3{\cdot}9H_2O$ with purity of 98.5% and SEP (each with 3 g) was first immersed in deionized water (100 mL) and then stirred with a

https://doi.org/10.1021/acssuschemeng.2c06739
ACS Sustainable Chem. Eng. XXXX, XXX, XXX−XXX

magnetic stirring bar at 900 revolutions per minute (rpm) for 12 h at a temperature of 40 °C until the solid chemicals dissolved completely. Second, the prepared solution was heated up to 80 °C for 4 h to evaporate most of the free water. The wet sample was then dried at 100 °C for 8 h in a drying oven. Last, the sample was calcinated at 550 °C for 5 h. The desired catalyst, Fe_2O_3-sepiolite (Fe_2O_3-SEP), was finally obtained. The same method was used to synthesize the CuO-sepiolite catalyst (CuO-SEP) in this work as well. More details for the preparation procedure of catalysts were also reported in our previous published work.[19] In addition, different techniques were used in this work to characterize the physicochemical properties of the prepared catalysts; the details can be found in our previous study, and the same method was also applied in this work.[19]

Experimental Measurements. In this work, 200 mL of 5 M aqueous MEA solution was used to prepare the CO_2-rich MEA solution by using the experimental setup described in the work of Zhang et al.[19], the CO_2 absorption process was performed at 40 °C with a CO_2 partial pressure of 100 kPa. The final CO_2 loading was determined by using the titration method with 1 M HCl solution,[41] and the obtained results indicated that the CO_2-rich loading was 0.590 mol CO_2/mol amine. Then, the prepared CO_2-rich MEA solution was used for all the CO_2 desorption experiments to evaluate the catalytic performance of the synthesized catalysts; the scheme for the experimental setup can also be found in our previous published work.[19] Desorption experiments were conducted on 200 mL of solution, with and without the catalysts, so as to have a reference under the same operating conditions (blank). In the catalyst-aided desorption experiments, 2.5 g of the catalyst was put into the three-necked flask reactor containing the CO_2-rich MEA solution (the mass ratio of catalyst to amine solution is 1.25:100). Desorption experiments were performed at the temperature of 100 °C with an oil bath, which was covered with insulating cotton (with a thickness of about 5 cm) to avoid the effect of room temperature. The desorbed CO_2 was carried at the pure N_2 gas stream (500 mL/min), and its concentration was analyzed with an infrared CO_2 analyzer (COZIR-100, ±0.01% in accuracy, GSS Ltd., UK) and recorded by computer with an interval time of 10 s. Here, the CO_2 loading in the liquid gas can be calculated based the obtained CO_2 concentration in the outlet gas at each record time; the details for the calculation method can be found in the work of Zhang et al.[41]

In addition, to better understand the reaction mechanism, the speciation for the CO_2-loaded MEA solution at different CO_2 loadings was analyzed by using a nuclear magnetic resonance (NMR) spectrometer (Bruker Avance III 400) at a temperature of 25 °C. The NMR analysis conditions and sample preparation method involved in this work were the same as those used and validated in our previous work.[42]

Parameters for Evaluating the Catalytic Performance. To evaluate and compare the catalytic CO_2 desorption performances of the synthesized catalysts, a series of parameters such as CO_2 desorption rate (V_d, mol-CO_2/(mol-amine·min)), CO_2 desorption capacity (n, mole), and heat duty (H, kJ/mol-CO_2) were selected and calculated as shown in eqs 1−3, respectively.[19]

$$V_d = \frac{\frac{V_{N_2} \times C'}{1 - C'} \times \frac{273.15}{V_m \times T}}{C \times V} \quad (1)$$

$$n_{CO_2} = (\alpha_{rich} - \alpha_{lean}) \times V \quad (2)$$

$$H = \frac{\text{heat input/time}}{\text{CO}_2\text{ amount/time}} = \frac{E\ (\text{kJ})}{n_{CO_2}(\text{mol})} \quad (3)$$

where V_{N_2} is the flow rate of the carrier gas, in N_2; C' is the concentration of CO_2 in the exit gas mixture, in mol%; V_m is the standard molar volume of gases, at 22.4 L/mol; T is the room temperature, in kelvin; C is the concentration of the MEA solution, at 5 mol/L; V is the volume of the MEA solution in the reactor, at 0.2 L; α_{rich} is the CO_2-rich loading, in mol-CO_2/mol-amine; α_{lean} is the CO_2-lean loading, in mol-CO_2/mol-amine; E is the recorded electricity consumption, in kJ; and n_{CO_2} is the CO_2 desorption capacity in moles.

The heat duty (eq 3) measured in this work is defined as the heat required for the release of 1 mol of CO_2, and it can be described by the ratio between the heat input and the amount of desorbed CO_2 using a widely accepted approach.[24,43−45] In this work, heat consumption for sorbent regeneration was reported as electricity consumption measured using a digital electric meter (Zhejiang Tepsung Electric Co., Ltd.) for the entire duration of the desorption process; this method, commonly used in laboratory-scale testing, allows for a reasonable comparison to evaluate the catalytic performance of different catalysts in a single work for each parallel test.

It should be noted, however, that the obtained values of these parameters can only be used in this work for comparison purposes, since a relatively low temperature was applied in this work to provide a relatively slow CO_2 desorption rate, which can amplify the differences between the various catalytic systems.

The relative desorption energy consumption (RH, eq 4) was also used to compare the catalytic performances of the catalysts studied in this work.[46] In addition, the desorption factor (DF, $mol^3/(kJ \cdot min)$) was adopted to further correlate the structure−activity relationship between the catalyst and the CO_2 desorption performance, as shown in eq 5:[19]

$$\text{RH}(\%) = \frac{H_i}{H_0} \times 100 \quad (4)$$

$$\text{DF} = \frac{V_d \times n_{CO_2}}{H_i} \quad (5)$$

where H_i and H_0 are the heat duty in the solvent regeneration process with and without the catalyst, respectively.

RESULTS AND DISCUSSION

Desorption Performance of the Catalyst. In this work, the catalytic CO_2 desorption performances of Fe_2O_3-SEP and CuO-SEP in CO_2-loaded MEA solutions were investigated by determining the desorption rate, desorption capacity, and relative energy consumption during regeneration processes conducted at 100 °C with a mass ratio of catalyst to amine solution of 1.25:100. Figure 2 displays the changes in the relative CO_2 loadings in the amine solution with and without catalysts. It clearly shows that the CO_2 that remained in the

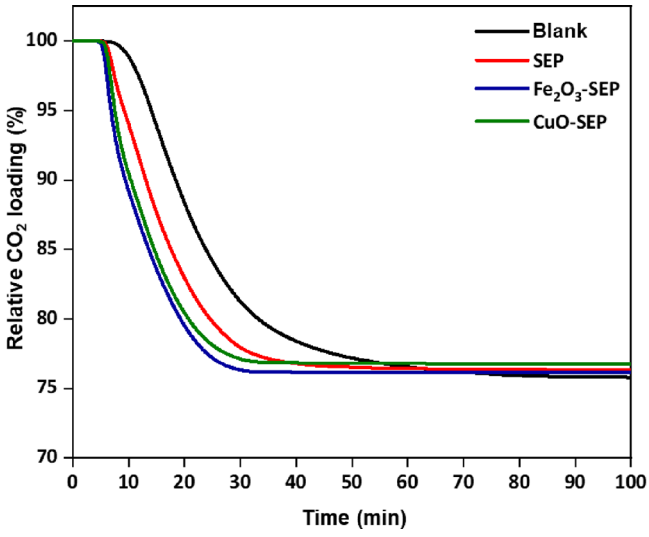

Figure 2. Comparison of CO_2 releasing rates with and without catalysts.

https://doi.org/10.1021/acssuschemeng.2c06739
ACS Sustainable Chem. Eng. XXXX, XXX, XXX−XXX

MEA solution decreases rapidly at the desorption time between 10 and 30 min. The final CO_2 loadings for all systems are almost the same, indicating that the CO_2 desorption processes finally reach an equilibrium state. This also demonstrates that the addition of a catalyst can only accelerate the CO_2 desorption rate but not change the chemical equilibrium of the desorption reaction.

Figure 2 also demonstrates that the CO_2 desorption starts earlier with all tested catalysts than with the non-catalytic MEA solution (blank). The activity for CO_2 releasing decreases in the order Fe_2O_3-SEP > CuO-SEP > SEP > blank. The metal oxides loaded on the SEP carrier might behave as an active site to catalyze the CO_2 desorption, and the Fe_2O_3-SEP catalyst performs better than others tested in this work.

As mentioned in our previous works,[13,19] the CO_2 desorption performance can be assessed by the CO_2 desorption rate, the amount of desorbed CO_2, and the energy consumption, calculated from the data acquired in the first 20 mins of the desorption experiments, because the CO_2 loading drops rapidly in the first 10−30 mins during the CO_2 desorption process and then slows down, as shown in Figure 2. Figure 3 illustrates the desorption performances in different

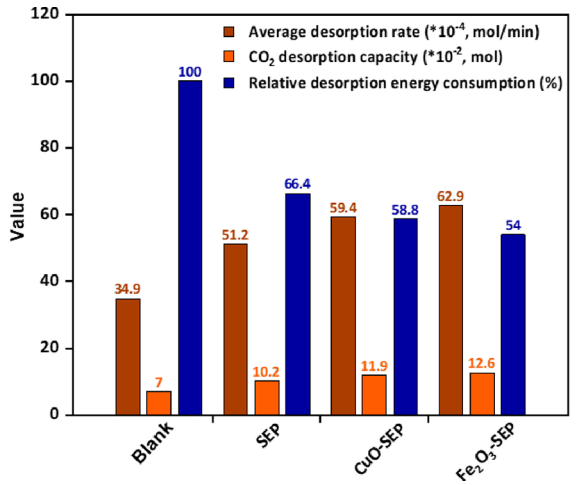

Figure 3. Comparison of the CO_2 desorption performances of SEP-based catalysts.

CO_2-loaded MEA solutions with and without catalysts, in terms of average CO_2 desorption rate, desorption capacity, and relative desorption energy consumption. The results showed that the average CO_2 desorption rate ($\times 10^{-4}$ mol/min) decreased in the order Fe_2O_3-SEP (62.9) > CuO-SEP (59.4) > SEP (51.2) > blank (34.9), and the same trend was also found for the CO_2 desorption capacity ($\times 10^{-2}$ mol), i.e., Fe_2O_3-SEP (12.6) > CuO-SEP (11.9) > SEP (10.2) > blank (7.0). In contrast, the relative desorption energy consumption RH (%) followed the order blank (100) > SEP (66.4) > CuO-SEP (58.8) > Fe_2O_3-SEP (54.0). Figure 3 shows that, for the MEA system, the addition of a catalyst can accelerate the CO_2 desorption rate by 46.7−166.2%, increase the CO_2 desorption capacity by 45.7−80.0%, and reduce the energy demand by 33.6−46.0%. Therefore, the CO_2 desorption efficiency in the MEA regeneration process can be significantly improved with the addition of SEP-based catalysts, among which the best results can be obtained with Fe_2O_3-SEP.

Table 1 illustrates a comparison of the catalytic CO_2 desorption performance between the catalysts prepared in this work and others reported in the literature. The reported desorption performance data refer to the use of the indicated catalyst in CO_2-loaded solutions of 5 M MEA. As evident, the use of solid acid catalysts generally results in an increase in the amount of CO_2 desorbed (values greater than 0%) and a decrease in relative heat duty (percentages less than 100%) compared to 5 M MEA desorbed in the absence of any catalyst. It is worth noting that all experimental data reported in Table 1 refer to a desorption temperature ≤100 °C, which is significantly lower than that of the conventional process (120−140 °C): this lower temperature, which is possible precisely because of the use of catalysts, helps to effectively reduce the heat of evaporation for solvent regeneration and thus promote the reduction of the heat duty.

Table 1. CO_2 Catalytic Desorption Performance of Different Catalysts when Added to CO_2-Loaded 5 M MEA Solution[a]

catalysts	desorption temperature (°C)	increase in desorbed CO_2 amount (%)	relative heat duty (%)	reference
SEP	100	46	66.4	this work
CuO-SEP	100	70	58.8	
Fe_2O_3-SEP	100	80	54	
KIT-6	100	31	79.8	
Cr-Mont	86	26.2	79.1	33
Co-Mont	86	45.5	67.6	
Fe-Mont	86	82.4	60	
CuO-KIT-6	100	49	66.6	19
NiO-KIT-6	100	32	75.4	
Fe_2O_3-KIT-6	100	34	76.5	
SO_4^{2-}/ZIF-67-C@ TiO_2	88	65	64	16
SO_3H-MCM-41	90	53	68	44
Al_2O_3-HZSM-5	96	38	66	47
SO_4^{2-}/ZrO_2-Al_2O_3	98	34	62	28
SO_4^{2-}/ZrO_2-SiO_2	97	40	64	27
CMK-3-SBA-15	97	6.9	78.5	48
CMK-3-MCM-41	97	17.2	69.7	
CMK-3-SiO_2	97	69	62.6	
Ce-M-HPW-15	88	38.1	70.5	49
SAPO-34	96	28.1	75.7	23
SO_4^{2-}/ZrO_2-HZSM-5	98	40	69	24

[a]Percentages refer to increases or decreases from values obtained under the same operating conditions by desorbing MEA without using catalysts.

Although the catalytic desorption performances were determined under conditions that were not always homogeneous with each other (due to different dosages of the catalysts used, desorption temperature, stirring, or total desorption time), the comparison shown in Table 1 highlights the potential advantages of SEP-based catalysts: their high performance, combined with important features such as low cost and environmental compatibility, indicating that SEP-based catalysts deserved to be further studied in the future. In particular, the enormous reduction in energy consumption for solvent regeneration achieved in this work for CuO-SEP and Fe_2O_3-SEP catalysts can significantly reduce the operating cost, further encouraging the industrial application of amine-based carbon capture technology.

Catalyst Characterization and Structure−Activity Relationship. Figure 4 presents the wide-angle XRD patterns of three catalysts (SEP, Fe_2O_3-SEP, CuO-SEP) in the range of

https://doi.org/10.1021/acssuschemeng.2c06739
ACS Sustainable Chem. Eng. XXXX, XXX, XXX−XXX

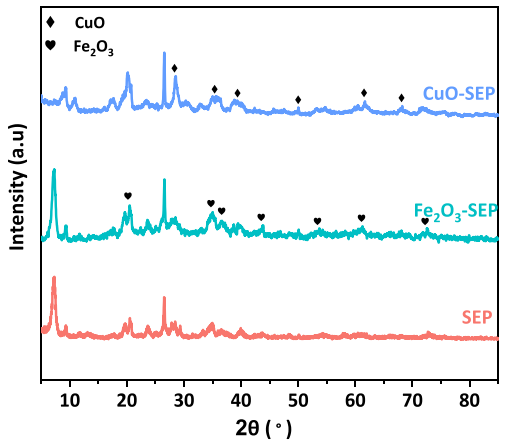

Figure 4. X-ray diffractograms of SEP-based catalysts.

5 to 90°. The characteristic diffraction peaks of SEP usually appear at 7.2, 20.6, 26.5, 27.9, 35.0, and 39.9°, respectively.[50] It is observed that the main characteristic peaks of all samples did not change significantly compared to the SEP carrier, which indicates that the samples still retain their original crystal structure after loading metal oxides. The characteristic diffraction peaks of Fe_2O_3-SEP at 35.6, 40.8, 54.1, 62.3, and 63.8° correspond to α-Fe_2O_3.[51,52] CuO-SEP generates characteristic diffraction peaks at 35.5, 38.6, 48.6, 62.4, and 66.2°, respectively.[53] These profiles demonstrate that the metal oxides were loaded on the SEP carrier successfully and without affecting the crystal structure of SEP.

The FT-IR spectra of the three SEP-based catalysts are shown in Figure 5. It is observed that the three catalysts show

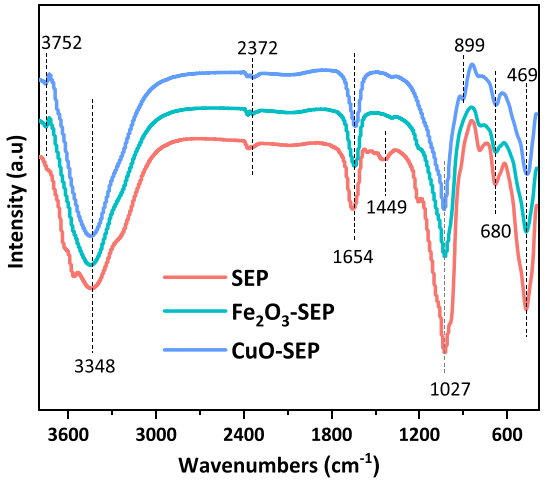

Figure 5. FT-IR spectra of SEP-based catalysts.

similar IR spectra, with absorption peaks at 3348 and 1654 cm^{-1} attributable to the stretching vibration of the hydroxyl group in SEP, which is caused by the presence of zeolite and combined water, respectively, in the SEP structure. The characteristic absorption peaks at 1027 and 469 cm^{-1} are caused by the antisymmetric stretching vibration of the Si−O bond and the bending vibration of the Si−O−Si bond on the SEP tetrahedral silicon wafer.[54,55] The absorption peak at 1027 cm^{-1} is still present after loading metal oxides, which proves that the basic structure of SEP has not changed. The decreased width of absorption peaks at 3348 and 1027 cm^{-1} indicates the presence of metal oxides in the SEP structure, while the appearance of new absorption peaks at 3752 and 899 cm^{-1} indicates the presence of new substances in SEP. FT-IR results show that part of the structure of SEP was retained and the metal oxides were completely dispersed on the surface or skeleton of SEP. Based on the obtained characteristic results, it is concluded that the Fe_2O_3-SEP catalyst retains the best SEP structure, in great agreement with the XRD results.

The adsorption−desorption isotherms and the BET-specific surface area of SEP can be obtained by N_2 adsorption−desorption experiments to analyze the internal changes of SEP before and after metal oxide loading. Figure 6 presents that the N_2 adsorption−desorption curves of supported SEP catalysts belong to class IV adsorption−desorption isotherms with a type H3 hysteresis loop according to the catalyst classification prescribed by the International Union of Pure and Applied Chemistry (IUPAC). This indicates that all catalysts in Figure 6 contain slit-like pore structures. The isotherms of the three catalysts with little difference suggest that SEP retains its original structure after loading metal oxides, which is consistent with the results of XRD and FT-IR.

The structure and physical properties of the three SEP catalysts are listed in Table 2, including the BET-specific surface area, pore volume, and pore size. The intermediary pore area was calculated as the BET surface area minus the *t*-plot micropore area. It is observed that the specific surface area and pore volume of SEP decrease with the load of metal oxides, but the pore size increases after the load, which may be caused by calcination at high temperature. The mesoporous surface area (MSA) of the three catalysts decreases in the order SEP > Fe_2O_3-SEP > CuO-SEP. A higher MSA and a larger pore size allow more acid sites (Brønsted and Lewis acid) to be exposed to ions in CO_2-rich solution, especially $MEAH^+$ and $MEACOO^-$, and the interaction between the acid sites and each ion increases to the benefit of the CO_2 desorption process.

The pyridine infrared spectroscopy (Py-IR) spectra of the tested catalysts are shown in Figure 7. The characteristic absorption peaks of the Py-IR spectra at 1540 and 1450 cm^{-1} represent Brønsted and Lewis acid sites, respectively. The intensity of the peak at 1540 cm^{-1} is smaller, indicating that the content of Brønsted acid sites in the SEP catalyst is lower. The concentrations of the Brønsted and Lewis acid sites as well as the B/L ratios are summarized in Table 3. It is observed that the Brønsted acid content of the three catalysts follows the order Fe_2O_3-SEP > CuO-SEP > SEP, while the Lewis acid contents in the order SEP > CuO-SEP > Fe_2O_3-SEP. In addition, the ratio of the Brønsted and Lewis acid sites (B/L) decreases in the order Fe_2O_3-SEP > CuO-SEP > SEP. It has been revealed that more Brønsted acid sites and a higher B/L ratio benefit the catalytic performance for CO_2 desorption,[19] which is in agreement with the CO_2 desorption performances shown in Figure 3. Since Fe_2O_3 supported on SEP has a higher content of the Brønsted acid site and B/L ratio than CuO, it should be more competitive in the CO_2 desorption process.

For the catalytic CO_2 desorption process, the physical and chemical properties of the catalyst affect its catalytic performance, such as the CO_2 desorption rate, the amount of desorbed CO_2, and the heat duty. The DF, as an evaluating parameter as defined in eq 5, has been widely used to simply compare the CO_2 desorption performance in different amine systems with and without catalysts:[23,46] a higher value of DF indicates a better CO_2 desorption performance. To further understand the

https://doi.org/10.1021/acssuschemeng.2c06739
ACS Sustainable Chem. Eng. XXXX, XXX, XXX−XXX

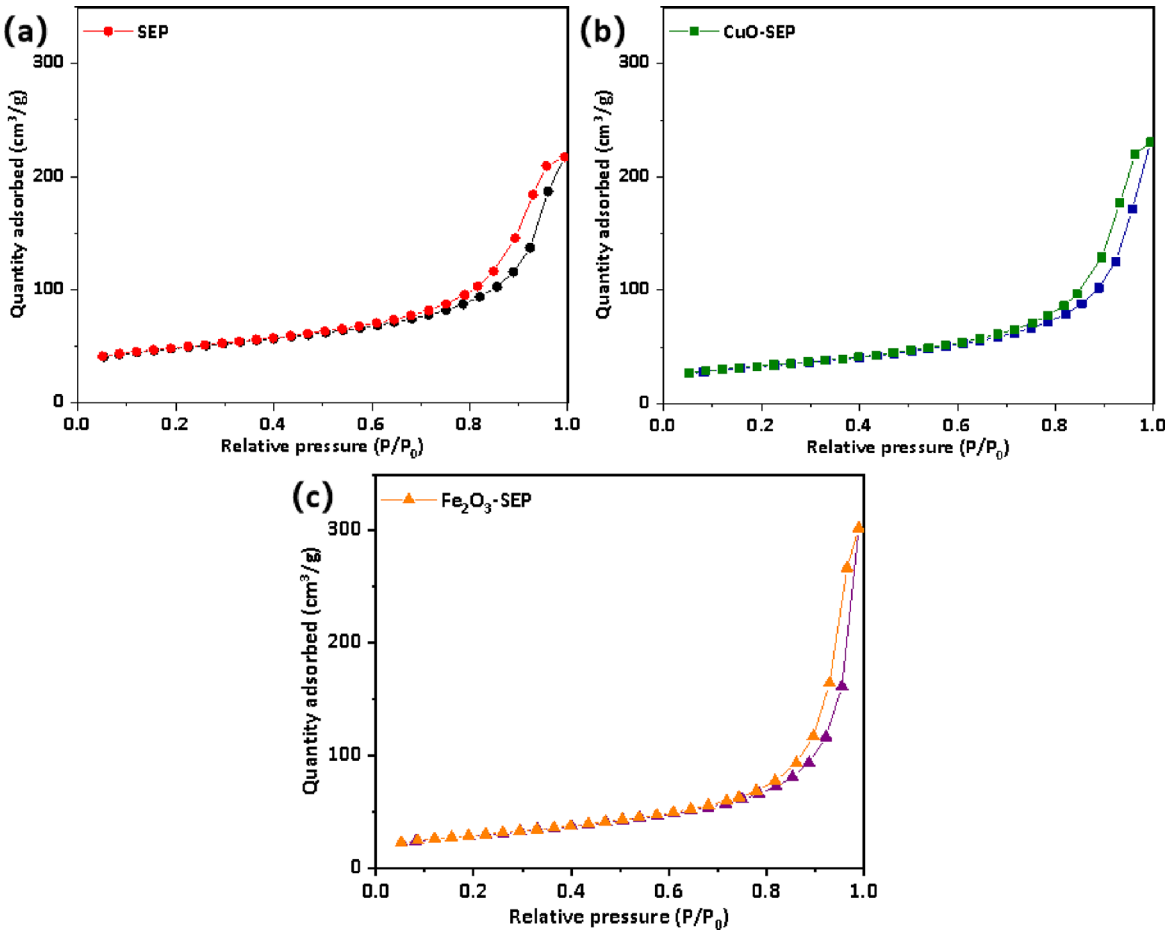

Figure 6. N_2 adsorption−desorption curves for the catalysts of (a) SEP, (b) CuO-SEP, and (c) Fe_2O_3-SEP.

Table 2. Structure and Physical Properties of SEP-Based Catalysts

	specific surface area (m^2/g)				
catalyst	sum	mesoporous	microporous	pore volume (cm^3/g)	pore size (nm)
SEP	159.2	101	58.2	0.27	11.8
CuO-SEP	112.4	86.5	25.9	0.25	14.4
Fe_2O_3-SEP	101.0	90	11.0	0.22	19.2

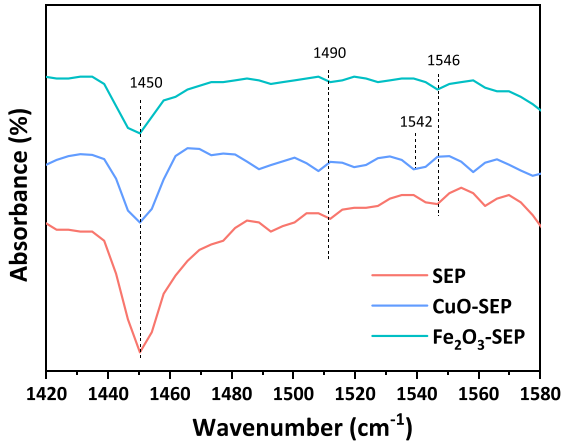

Figure 7. Py-IR profiles of SEP-based catalysts.

Table 3. Acidity Analysis of SEP-Based Catalysts

catalyst	Brønsted acid site (mmol/g)	Lewis acid site (mmol/g)	B/L ratio
SEP	0.04	0.90	0.05
CuO-SEP	0.06	0.53	0.12
Fe_2O_3-SEP	0.08	0.36	0.23

catalytic performance of SEP-based catalysts for CO_2 release, the DF (mol^3/(kJ·min)) was correlated with physicochemical properties (MSA, Brønsted acid site content, B/L ratio, etc.), as shown in Figure 8. As displayed in Figure 8a, even though MSA decreased after loading metal oxides on SEP, the catalytic CO_2 performance of metal oxide-supported SEP was enhanced, confirming that the metal oxides improved the catalytic activity of single SEP catalysts. Among the metal oxide-modified SEP catalysts, Fe_2O_3-SEP demonstrates a larger MSA and a better catalytic performance than CuO-SEP, which means that a larger MSA of the metal oxide-modified SEP catalyst is beneficial to improving the catalytic performance for CO_2 desorption. In addition, as observed in Figure 8b,c, the catalytic CO_2 desorption performances of the catalysts increase with the Brønsted acid site content and B/L ratio, i.e., the higher the number of Brønsted acid sites, the better the catalytic performance. This may be contributed by two characteristics of the catalyst: A larger MSA allows the acidic Brønsted and Lewis sites to be more easily reached by ions from the CO_2-rich solution. Moreover, not only does the Brønsted acid site (SEP-OH) contribute to transfer its own

https://doi.org/10.1021/acssuschemeng.2c06739
ACS Sustainable Chem. Eng. XXXX, XXX, XXX−XXX

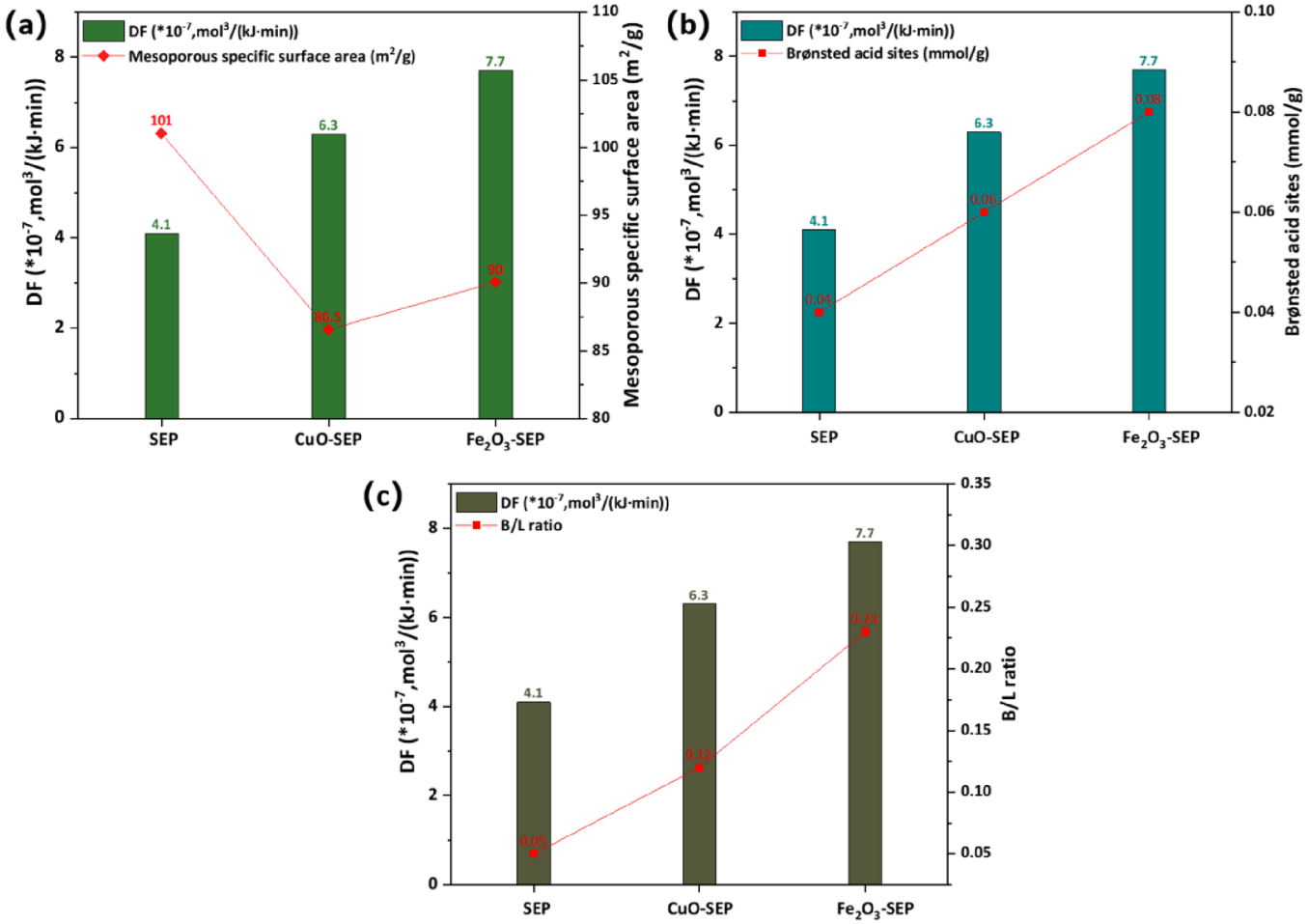

Figure 8. Relationship between the DF and physicochemical properties of catalysts including (a) mesopore-specific surface area, (b) content of Brønsted acid sites, and (c) B/L ratio.

proton to HCO_3^- and $MEACOO^-$ to release CO_2 but also its conjugate base ($SEP\text{-}O^-$) can act as a proton carrier from $MEAH^+$ to $MEACOO^-$ to promote the $MEAH^+$ deprotonation; both of the above behaviors cause the Brønsted acid site to play an important role in the catalytic CO_2 desorption process.

Catalytic Desorption Mechanism. As reported in many published works,[14,15,23,46] the regeneration process of MEA solution (CO_2 desorption) includes the decomposition of carbamate (breakdown of the N−C bond) and the deprotonation of protonated amine ($MEAH^+$).[56] The high energy requirement in solvent regeneration is mainly caused by the deprotonation of $MEAH^+$, as the CO_2-loaded amine solution still presents an alkaline environment with lack of H^+. This reaction is therefore endothermic; that is, it requires an external heat input.

In this work, the chemical species present in solution at different CO_2 loadings were identified and quantified by using the ^{13}C NMR technique,[57] and the results are plotted in Figure 9. Consistent with the literature and our previous studies, $MEAH^+$, $MEACOO^-$, and HCO_3^- are the dominant species at high CO_2 loading (>0.5).[58,59] At the very beginning of the CO_2 desorption process, HCO_3^- acts as a catalyst to obtain H^+ from the $MEAH^+$ and then form H_2CO_3 (R1); in addition, HCO_3^- can also subtract the proton from the hydroxyl group (SEP-OH) on the layered structure of the SEP-based catalyst (R2) to form H_2CO_3 and the conjugated base ($SEP\text{-}O^-$),

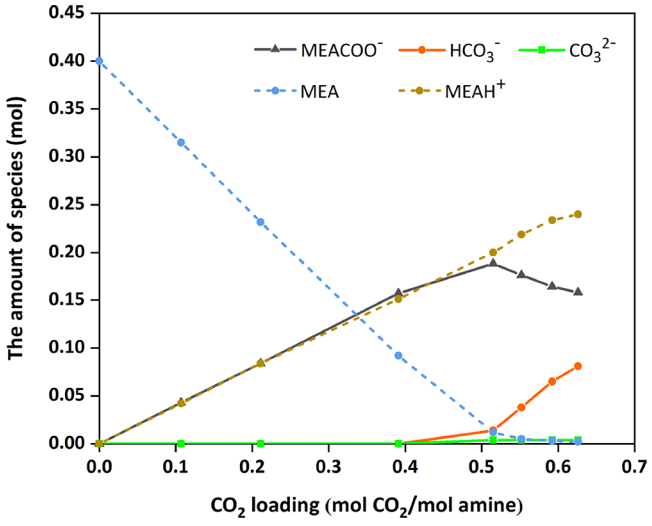

Figure 9. ^{13}C NMR speciation analysis as a function of the CO_2 loading.

which in turn accelerate the deprotonation of $MEAH^+$ (R3). This proton transformation process can complete the $MEAH^+$ deprotonation reaction and release CO_2 via the decomposition of H_2CO_3 by heating (R4), as HCO_3^- is not stable when it is heated at the temperature of 100 °C. On the other hand, the

https://doi.org/10.1021/acssuschemeng.2c06739
ACS Sustainable Chem. Eng. XXXX, XXX, XXX−XXX

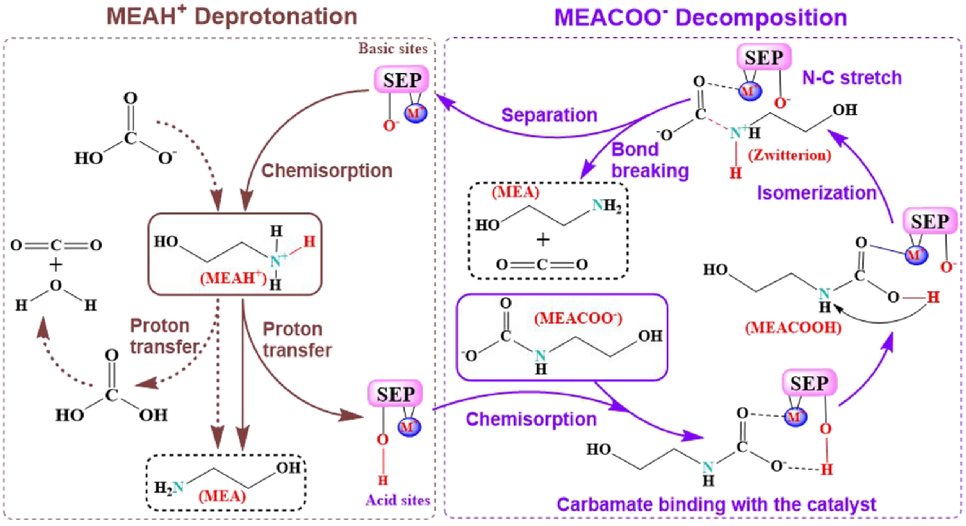

Figure 10. The pathways of $MEAH^+$ deprotonation and $MEACOO^-$ decomposition in the catalyst-aided desorption process for MEA.

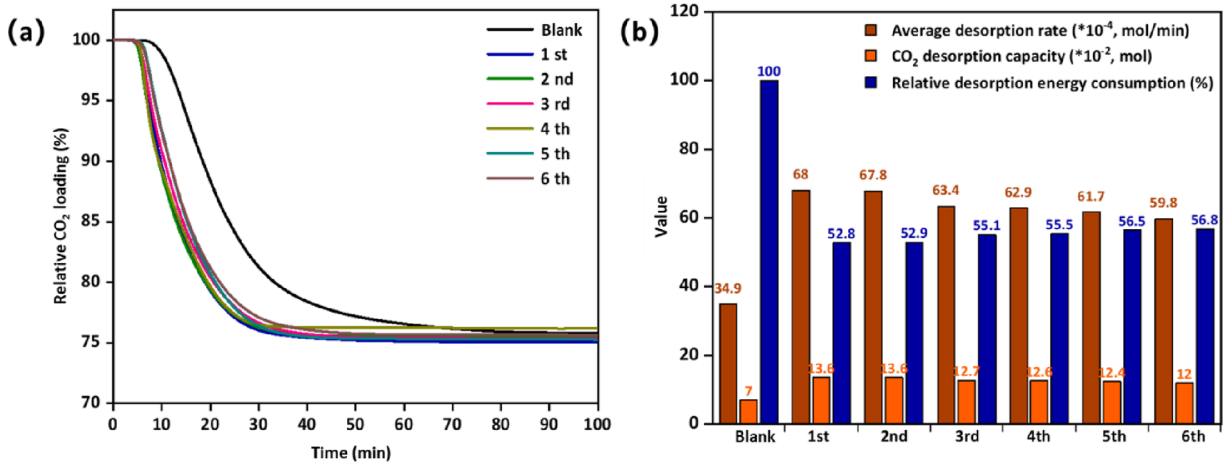

Figure 11. Cyclic stability test of the Fe_2O_3-SEP catalyst, including (a) relative CO_2 loading changing curves and (b) catalytic CO_2 desorption performance.

work of Shi et al.[43] proved that more heat is required for breaking the C−N bond of carbamate than for breaking the C−O bond of HCO_3^- to release CO_2. As a result, HCO_3^- is consumed quickly at the early stage of the CO_2 desorption.

$$MEAH^+ + HCO_3^- \rightarrow MEA + H_2CO_3 \quad (R1)$$

$$SEP - OH + HCO_3^- \rightarrow SEP - O^- + H_2CO_3 \quad (R2)$$

$$SEP - O^- + MEAH^+ \rightarrow MEA + SEP - OH \quad (R3)$$

$$H_2CO_3 \rightarrow CO_2 + H_2O \quad (R4)$$

Subsequently, a large amount of heat is still required for continuous CO_2 desorption from $MEACOO^-$ decomposition. However, catalysts can accelerate this process mainly due to Brønsted and Lewis acid sites on the catalyst surface.[13,19] In this work, the SEP surface was modified with the metal oxides CuO and Fe_2O_3, which are able to act predominantly as Lewis acids due to the unsaturated metal atoms that exist as it can accept the electron pair,[39] so the metal oxide (CuO and Fe_2O_3) in this work is expected to predominately act as a Lewis acidity. On the other hand, SEP itself has different "kinds" of water (Figure 1) that can convert to the hydroxyl group, which can subsequently provide the proton to bases such as HCO_3^- or $MEACOO^-$ to release CO_2: therefore, it can be concluded that the SEP can be regarded as a Brønsted acid site (donating protons).

The regeneration mechanism of CO_2-loaded aqueous MEA with SEP-based catalysts is shown in Figure 10, where M represents the unsaturated metal atoms on the SEP catalyst. Through a chemisorption process, the conjugated base (SEP-O^-) of Brønsted acid obtains the proton from $MEAH^+$ to release MEA; subsequently, SEP-OH can transfer the proton onto the oxygen of $MEACOO^-$ (forming MEACOOH), and then the proton moves from the O atom to the N atom through isomerization (forming the zwitterionic form $MEAH^+COO^-$). Meanwhile, Lewis acid accepts the lone electron pairs on the O and N atoms of $MEAH^+COO^-$ and then stretches the C−N bond to facilitate its decomposition, resulting in the release of MEA and CO_2. This catalyst-assisted proton transfer process, due to the synergistic work of the Brønsted and Lewis acid sites, facilitates the $MEAH^+$ deprotonation and the $MEACOO^-$ decomposition, lowering their activation energies, thus allowing the CO_2 desorption with a lower energy input, in agreement with the obtained results shown in Figure 3.

https://doi.org/10.1021/acssuschemeng.2c06739
ACS Sustainable Chem. Eng. XXXX, XXX, XXX−XXX

Stability Evaluation of the Catalyst. High stability is a very important property for catalysts, which determines the recycling efficiency for solvent regeneration, especially in industrial-scale applications. In this work, the Fe_2O_3-SEP catalyst was used for six consecutive catalytic desorption experiments with CO_2-loaded MEA solutions to verify its stability over time under the operating conditions used; the results of these recycling tests are shown in Figure 11, compared with desorption results obtained without a catalyst (blank). The change in CO_2 loading as a function of desorption time is shown in Figure 11a, which clearly shows that all processes conducted with the Fe_2O_3-SEP catalyst, even after six reuses, decreased the residual amount of CO_2 in solution more rapidly than the blank. Figure 11b shows that the Fe_2O_3-SEP catalyst maintains high catalytic activity, with no significant decay effect, even after six consecutive uses. Fresh Fe_2O_3-SEP (first) reduced the energy consumption for CO_2 desorption to 52.8% compared to the MEA solution without a catalyst, while after the catalyst was recycled six times (sixth), the energy consumption for CO_2 desorption was still reduced to 56.8%, which is only 4.0% higher than the first time. In addition, Figure 11b also displays that the amount of desorbed CO_2 is almost the same for all cycles: 0.136 mol of CO_2 was released with the fresh catalyst and 0.120 mol of CO_2 can still be desorbed at the sixth reuse. Meanwhile, the average CO_2 desorption rate ($\times 10^{-4}$ mol/min) decreases from 68 to 59.8 after the six cyclic tests, which means that less CO_2 is released with a slower desorption rate when cyclically using the catalyst, which leads to increased heat consumption. In summary, after six successive reuses, the Fe_2O_3-SEP catalyst still has an acceptable catalytic efficiency for CO_2 desorption. The reduced energy consumption can significantly save the operating cost for post-combustion CO_2 capture.

CONCLUSIONS

In this work, the low-cost environmentally friendly SEP was selected as an efficient catalyst carrier, and two metal oxide catalysts supported by SEP (Fe_2O_3-SEP and CuO-SEP) were synthesized by the impregnation method. Analysis of the catalytic CO_2 desorption performances of SEP, Fe_2O_3-SEP, and CuO-SEP in MEA solution led to the following conclusions:

(1) Compared with the blank experiment, the addition of catalysts can effectively reduce the energy consumption for CO_2 desorption, accelerate the CO_2 desorption rate, and increase the amount of the released CO_2. Among the tested catalysts, Fe_2O_3-SEP shows the best catalytic performance. The calculated relative desorption energy consumption (RH, %) decreased in the order blank (100) > SEP (66.4) > CuO-SEP (58.8) > Fe_2O_3-SEP (54.0).

(2) The characterization of catalysts revealed that a large mesoporous specific surface area and more Brønsted acid sites enhance the catalytic CO_2 desorption performance.

(3) Stability tests conducted on the Fe_2O_3-SEP catalyst demonstrated that its high performance in CO_2 desorption processes was maintained even at the sixth consecutive reuse. Overall, the metal oxide catalysts supported by SEP can effectively promote the CO_2 desorption at a lower temperature, thus reducing the desorption energy consumption for the CO_2 capture process with amine-based solution. SEP is a natural clay material that deserves further investigation and application in industry as a green, environmentally-friendly, and efficient catalyst carrier for catalytic CO_2 desorption.

AUTHOR INFORMATION

Corresponding Authors

Rui Zhang − *College of Chemical Engineering, Xiangtan University, Xiangtan, Hunan 411105, P.R. China;* orcid.org/0000-0003-4469-7594; Email: ruizhang@xtu.edu.cn, tange1026@163.com

Francesco Barzagli − *ICCOM Institute, National Research Council, 50019 Florence, Italy;* orcid.org/0000-0002-5077-0420; Email: francesco.barzagli@iccom.cnr.it

Zhien Zhang − *William G. Lowrie Department of Chemical and Biomolecular Engineering, The Ohio State University, Columbus, Ohio 43210, United States;* orcid.org/0000-0001-8594-6732; Email: zhienzhang@hotmail.com, zhang.4528@osu.edu

Authors

Yufan Li − *College of Chemical Engineering, Xiangtan University, Xiangtan, Hunan 411105, P.R. China*

Yiming Zhang − *College of Chemical Engineering, Xiangtan University, Xiangtan, Hunan 411105, P.R. China*

Ting Li − *College of Chemical Engineering, Xiangtan University, Xiangtan, Hunan 411105, P.R. China*

Luning Yang − *College of Chemical Engineering, Xiangtan University, Xiangtan, Hunan 411105, P.R. China*

Chao'en Li − *CSIRO Energy, Clayton North, Victoria 3169, Australia;* orcid.org/0000-0003-4233-3172

Complete contact information is available at: https://pubs.acs.org/10.1021/acssuschemeng.2c06739

Notes

The authors declare no competing financial interest.

ACKNOWLEDGMENTS

The work was supported by the National Natural Science Foundation of China (22008204), the China Postdoctoral Science Foundation (2021 M692704), and the Research Start-up Foundation of Xiangtan University (21QDZ56).

REFERENCES

(1) Bui, M.; Adjiman, C. S.; Bardow, A.; Anthony, E. J.; Boston, A.; Brown, S.; Fennell, P. S.; Fuss, S.; Galindo, A.; Hackett, L. A.; Hallett, J. P.; Herzog, H. J.; Jackson, G.; Kemper, J.; Krevor, S.; Maitland, G. C.; Matuszewski, M.; Metcalfe, I. S.; Petit, C.; Puxty, G.; Reimer, J.; Reiner, D. M.; Rubin, E. S.; Scott, S. A.; Shah, N.; Smit, B.; Trusler, J. P. M.; Webley, P.; Wilcox, J.; Mac Dowell, N. Carbon capture and storage (CCS): the way forward. *Energy Environ. Sci.* **2018**, *11*, 1062−1176.

(2) Liu, H.; Jiang, X.; Idem, R.; Dong, S.; Tontiwachwuthikul, P. AI models for correlation of physical properties in system of 1DMA2P-CO_2-H_2O. *AIChE J.* **2022**, *68*, No. e17761.

(3) Liang, Z. H.; Rongwong, W.; Liu, H.; Fu, K.; Gao, H.; Cao, F.; Zhang, R.; Sema, T.; Henni, A.; Sumon, K.; Nath, D.; Gelowitz, D.; Srisang, W.; Saiwan, C.; Benamor, A.; al-Marri, M.; Shi, H.; Supap, T.; Chan, C.; Zhou, Q.; Abu-Zahra, M.; Wilson, M.; Olson, W.; Idem, R.; Tontiwachwuthikul, P. Recent progress and new developments in post-combustion carbon-capture technology with amine based solvents. *Int. J. Greenh. Gas Con.* **2015**, *40*, 26−54.

(4) He, X.; He, H.; Barzagli, F.; Amer, M. W.; Li, C. e.; Zhang, R. Analysis of the energy consumption in solvent regeneration processes

using binary amine blends for CO_2 capture. *Energy* **2023**, *270*, No. 126903.
(5) Yu, Y.; Shen, Y.; Zhou, X.; Liu, F.; Zhang, S.; Lu, S.; Ye, J.; Li, S.; Chen, J.; Li, W. Relationship between tertiary amine's physical property and biphasic solvent's CO_2 absorption performance: Quantum calculation and experimental demonstration. *Chem. Eng. J.* **2022**, *428*, No. 131241.
(6) Shen, Y.; Liu, F.; Wang, X.; Shao, P.; He, Z.; Zhang, S.; Chen, L.; Li, S.; Li, W.; Wang, L.; Hou, Y. A pore matching amine-functionalized strategy for efficient CO_2 physisorption with low energy penalty. *Chem. Eng. J.* **2022**, *432*, No. 134403.
(7) Wang, L.; Zhang, Y.; Wang, R.; Li, Q.; Zhang, S.; Li, M.; Liu, J.; Chen, B. Advanced monoethanolamine absorption using sulfolane as a phase splitter for CO_2 Capture. *Environ. Sci. Technol.* **2018**, *52*, 14556−14563.
(8) Shao, P.; He, Z.; Hu, Y.; Shen, Y.; Zhang, S.; Yu, Y. Zeolitic imidazolate frameworks with different organic ligands as carriers for Carbonic anhydrase immobilization to promote the absorption of CO_2 into tertiary amine solution. *Chem. Eng. J.* **2022**, *435*, No. 134957.
(9) Dong, S.; Quan, H.; Zhao, D.; Li, H.; Geng, J.; Liu, H. Generic AI models for mass transfer coefficient prediction in amine-based CO_2 absorber, Part I: BPNN model. *Chem. Eng. Sci.* **2022**, *264*, No. 118165.
(10) Quan, H.; Dong, S.; Zhao, D.; Li, H.; Geng, J.; Liu, H. Generic AI models for mass transfer coefficient prediction in amine-based CO_2 absorber, Part II: RBFNN and RF model. *AIChE J.* **2023**, *69*, No. e17904.
(11) Chen, G.; Chen, G.; Peruzzini, M.; Barzagli, F.; Zhang, R. Investigating the performance of ethanolamine and benzylamine blends as promising sorbents for postcombustion CO_2 capture through ^{13}C NMR speciation and heat of CO_2 absorption analysis. *Energy Fuels* **2022**, *36*, 9203−9212.
(12) Zhang, R.; Zhang, X.; Yang, Q.; Yu, H.; Liang, Z.; Luo, X. Analysis of the reduction of energy cost by using MEA-MDEA-PZ solvent for post-combustion carbon dioxide capture (PCC). *Appl. Energy* **2017**, *205*, 1002−1011.
(13) Tan, Z.; Zhang, S.; Yue, X.; Zhao, F.; Xi, F.; Yan, D.; Ling, H.; Zhang, R.; Tang, F.; You, K.; Luo, H. a.; Zhang, X. Attapulgite as a cost-effective catalyst for low-energy consumption amine-based CO_2 capture. *Sep. Purif. Technol.* **2022**, *298*, No. 121577.
(14) Alivand, M. S.; Mazaheri, O.; Wu, Y.; Stevens, G. W.; Scholes, C. A.; Mumford, K. A. Catalytic solvent regeneration for energy-efficient CO_2 capture. *ACS Sustain. Chem. Eng.* **2020**, *8*, 18755−18788.
(15) de Meyer, F.; Bignaud, C. The use of catalysis for faster CO_2 absorption and energy-efficient solvent regeneration: An industry-focused critical review. *Chem. Eng. J.* **2022**, *428*, No. 131264.
(16) Xing, L.; Wei, K.; Li, Y.; Fang, Z.; Li, Q.; Qi, T.; An, S.; Zhang, S.; Wang, L. TiO_2 coating strategy for robust catalysis of the metal−organic framework toward energy-efficient CO_2 capture. *Environ. Sci. Technol.* **2021**, *55*, 11216−11224.
(17) Xing, L.; Li, M.; Li, M.; Xu, T.; Li, Y.; Qi, T.; Li, H.; Hu, Z.; Hao, G.-p.; Zhang, S.; James, T. D.; Mao, B.; Wang, L. MOF-derived robust and synergetic acid sites inducing C−N bond disruption for energy-efficient CO_2 desorption. *Environ. Sci. Technol.* **2022**, *56*, 17936−17945.
(18) Li, T.; Yu, Q.; Barzagli, F.; Li, C. e.; Che, M.; Zhang, Z.; Zhang, R. Energy efficient catalytic CO_2 desorption: mechanism, technological progress and perspective. *Carbon Capture Sci. Technol.* **2023**, *6*, No. 100099.
(19) Zhang, R.; Li, T.; Zhang, Y.; Ha, J.; Xiao, Y.; Li, C. e.; Zhang, X.; Luo, H. a. CuO modified KIT-6 as a high-efficiency catalyst for energy-efficient amine solvent regeneration. *Sep. Purif. Technol.* **2022**, No. 121702.
(20) Liu, F.; Huang, K.; Zheng, A.; Xiao, F.-S.; Dai, S. Hydrophobic solid acids and their catalytic applications in green and sustainable chemistry. *ACS Catal.* **2018**, *8*, 372−391.
(21) Liang, Z.; Idem, R.; Tontiwachwuthikul, P.; Yu, F.; Liu, H.; Rongwong, W. Experimental study on the solvent regeneration of a CO_2-loaded MEA solution using single and hybrid solid acid catalysts. *AIChE J.* **2016**, *62*, 753−765.
(22) Bhatti, U. H.; Ienco, A.; Peruzzini, M.; Barzagli, F. Unraveling the role of metal oxide catalysts in the CO_2 desorption process from nonaqueous sorbents: an experimental study carried out with ^{13}C NMR. *ACS Sustain. Chem. Eng.* **2021**, *9*, 15419−15426.
(23) Zhang, X.; Zhang, X.; Liu, H.; Li, W.; Xiao, M.; Gao, H.; Liang, Z. Reduction of energy requirement of CO_2 desorption from a rich CO_2-loaded MEA solution by using solid acid catalysts. *Appl. Energy* **2017**, *202*, 673−684.
(24) Xing, L.; Wei, K.; Li, Q.; Wang, R.; Zhang, S.; Wang, L. One-step synthesized SO_4^{2-}/ZrO_2-HZSM-5 solid acid catalyst for carbamate decomposition in CO_2 capture. *Environ. Sci. Technol.* **2020**, *54*, 13944−13952.
(25) Gao, H.; Huang, Y.; Zhang, X.; Bairq, Z. A. S.; Huang, Y.; Tontiwachwuthikul, P.; Liang, Z. Catalytic performance and mechanism of SO_4^{2-}/ZrO_2/SBA-15 catalyst for CO_2 desorption in CO_2-loaded monoethanolamine solution. *Appl. Energy* **2020**, *259*, No. 114179.
(26) Zhang, X.; Zhu, Z.; Sun, X.; Yang, J.; Gao, H.; Huang, Y.; Luo, X.; Liang, Z.; Tontiwachwuthikul, P. Reducing energy penalty of CO_2 capture using Fe promoted SO_4^{2-}/ZrO_2/MCM-41 catalyst. *Environ. Sci. Technol.* **2019**, *53*, 6094−6102.
(27) Ali Saleh Bairq, Z.; Gao, H.; Huang, Y.; Zhang, H.; Liang, Z. Enhancing CO_2 desorption performance in rich MEA solution by addition of $SO_4^{2-}/ZrO_2/SiO_2$ bifunctional catalyst. *Appl. Energy* **2019**, *252*, No. 113440.
(28) Zhang, X.; Hong, J.; Liu, H.; Luo, X.; Olson, W.; Tontiwachwuthikul, P.; Liang, Z. SO_4^{2-}/ZrO_2 supported on γ-Al_2O_3 as a catalyst for CO_2 desorption from CO_2-loaded monoethanolamine solutions. *AIChE J.* **2018**, *64*, 3988−4001.
(29) Nagendrappa, G. Organic synthesis using clay and clay-supported catalysts. *Appl. Clay Sci.* **2011**, *53*, 106−138.
(30) Jha, A.; Garade, A. C.; Shirai, M.; Rode, C. V. Metal cation-exchanged montmorillonite clay as catalysts for hydroxyalkylation reaction. *Appl. Clay Sci.* **2013**, *74*, 141−146.
(31) Bhatti, U. H.; Sultan, H.; Min, G. H.; Nam, S. C.; Baek, I. H. Ion-exchanged montmorillonite as simple and effective catalysts for efficient CO_2 capture. *Chem. Eng. J.* **2021**, *413*, No. 127476.
(32) Bhatti, U. H.; Kazmi, W. W.; Muhammad, H. A.; Min, G. H.; Nam, S. C.; Baek, I. H. Practical and inexpensive acid-activated montmorillonite catalysts for energy-efficient CO_2 capture. *Green Chem.* **2020**, *22*, 6328−6333.
(33) Bhatti, U. H.; Kazmi, W. W.; Min, G. H.; Haider, J.; Nam, S.; Baek, I. H. Facilely synthesized M-montmorillonite (M = Cr, Fe, and Co) as efficient catalysts for enhancing CO_2 desorption from amine solution. *Ind. Eng. Chem. Res.* **2021**, *60*, 13318−13325.
(34) Tan, Z.; Zhang, S.; Zhao, F.; Zhang, R.; Tang, F.; You, K.; Luo, H. a.; Zhang, X. SnO_2/ATP catalyst enabling energy-efficient and green amine-based CO_2 capture. *Chem. Eng. J.* **2023**, *453*, No. 139801.
(35) Choudhury, A.; Bhowmick, A. K.; Ong, C.; Soddemann, M. Influence of molecular parameters on thermal, mechanical, and dynamic mechanical properties of hydrogenated nitrile rubber and its nanocomposites. *Polym. Eng. Sci.* **2010**, *50*, 1389−1399.
(36) Chivrac, F.; Pollet, E.; Schmutz, M.; Avérous, L. Starch nano-biocomposites based on needle-like sepiolite clays. *Carbohydr. Polym.* **2010**, *80*, 145−153.
(37) Galan, E.; Carretero, M. I. A new approach to compositional limits for sepiolite and palygorskite. *Clays Clay Miner.* **1999**, *47*, 399−409.
(38) Mohd Zaini, N. A.; Ismail, H.; Rusli, A. Short review on sepiolite-filled polymer nanocomposites. *Polym.-Plast. Technol. Eng.* **2017**, *56*, 1665−1679.
(39) Bhatti, U. H.; Shah, A. K.; Kim, J. N.; You, J. K.; Choi, S. H.; Lim, D. H.; Nam, S.; Park, Y. H.; Baek, I. H. Effects of transition metal oxide catalysts on MEA solvent regeneration for the post-

https://doi.org/10.1021/acssuschemeng.2c06739
ACS Sustainable Chem. Eng. XXXX, XXX, XXX−XXX

combustion carbon capture process. *ACS Sustain. Chem. Eng.* **2017**, *5*, 5862−5868.
(40) Bhatti, U. H.; Nam, S.; Park, S.; Baek, I. H. Performance and mechanism of metal oxide catalyst-aided amine solvent regeneration. *ACS Sustain. Chem. Eng.* **2018**, *6*, 12079−12087.
(41) Zhang, R.; Zhang, Y.; Cheng, Y.; Yu, Q.; Luo, X.; Li, C.; Li, J.; Zeng, Z.; Liu, Y.; Jiang, X.; Hu, X. E. New approach with universal applicability for evaluating the heat requirements in the solvent regeneration process for postcombustion CO_2 capture. *Ind. Eng. Chem. Res.* **2020**, *59*, 3261−3268.
(42) Barzagli, F.; Peruzzini, M.; Zhang, R. Direct CO_2 capture from air with aqueous and nonaqueous diamine solutions: a comparative investigation based on ^{13}C NMR analysis. *Carbon Capture Sci. Technol.* **2022**, *3*, No. 100049.
(43) Shi, H.; Naami, A.; Idem, R.; Tontiwachwuthikul, P. Catalytic and non catalytic solvent regeneration during absorption-based CO_2 capture with single and blended reactive amine solvents. *Int. J. Greenh. Gas Con.* **2014**, *26*, 39−50.
(44) Sun, Q.; Li, T.; Mao, Y.; Gao, H.; Sema, T.; Wang, S.; Liu, L.; Liang, Z. Reducing heat duty of MEA regeneration using a sulfonic acid-functionalized mesoporous MCM-41 catalyst. *Ind. Eng. Chem. Res.* **2021**, *60*, 18304−18315.
(45) Bhatti, U. H.; Shah, A. K.; Hussain, A.; Khan, H. A.; Park, C. Y.; Nam, S. C.; Baek, I. H. Catalytic activity of facilely synthesized mesoporous HZSM-5 catalysts for optimizing the CO_2 desorption rate from CO_2-rich amine solutions. *Chem. Eng. J.* **2020**, *389*, No. 123439.
(46) Zhang, X.; Huang, Y.; Gao, H.; Luo, X.; Liang, Z.; Tontiwachwuthikul, P. Zeolite catalyst-aided tri-solvent blend amine regeneration: An alternative pathway to reduce the energy consumption in amine-based CO_2 capture process. *Appl. Energy* **2019**, *240*, 827−841.
(47) Zhang, X.; Liu, H.; Liang, Z.; Idem, R.; Tontiwachwuthikul, P.; Jaber Al-Marri, M.; Benamor, A. Reducing energy consumption of CO_2 desorption in CO_2-loaded aqueous amine solution using Al_2O_3/HZSM-5 bifunctional catalysts. *Appl. Energy* **2018**, *229*, 562−576.
(48) Ali Saleh Bairq, Z.; Gao, H.; Murshed, F. A. M.; Tontiwachwuthikul, P.; Liang, Z. Modified heterogeneous catalyst-aided regeneration of CO_2 capture amines: a promising perspective for a drastic reduction in energy consumption. *ACS Sustain. Chem. Eng.* **2020**, *8*, 9526−9536.
(49) Wei, K.; Xing, L.; Li, Y.; Xu, T.; Li, Q.; Wang, L. Heteropolyacid modified Cerium-based MOFs catalyst for amine solution regeneration in CO_2 capture. *Sep. Purif. Technol.* **2022**, *293*, No. 121144.
(50) Ye, Q.; Yan, L.; Wang, H.; Cheng, S.; Wang, D.; Kang, T.; Dai, H. Enhanced catalytic performance of rare earth-doped Cu/H-Sep for the selective catalytic reduction of NO with C_3H_6. *Appl. Catal., A* **2012**, *431-432*, 42−48.
(51) Cho, J. M.; Han, G. Y.; Jeong, H.-K.; Roh, H.-S.; Bae, J. W. Effects of ordered mesoporous bimodal structures of Fe/KIT-6 for CO hydrogenation activity to hydrocarbons. *Chem. Eng. J.* **2018**, *354*, 197−207.
(52) Xia, Y.; Dai, H.; Jiang, H.; Zhang, L.; Deng, J.; Liu, Y. Three-dimensionally ordered and wormhole-like mesoporous iron oxide catalysts highly active for the oxidation of acetone and methanol. *J. Hazard. Mater.* **2011**, *186*, 84−91.
(53) Subhan, F.; Aslam, S.; Yan, Z.; Ikram, M.; Rehman, S. Enhanced desulfurization characteristics of Cu-KIT-6 for thiophene. *Micropor. Mesopor. Mater.* **2014**, *199*, 108−116.
(54) Alkan, M.; Tekin, G.; Namli, H. FTIR and zeta potential measurements of sepiolite treated with some organosilanes. *Micropor. Mesopor. Mater.* **2005**, *84*, 75−83.
(55) Gao, Y.; Gan, H.; Zhang, G.; Guo, Y. Visible light assisted Fenton-like degradation of rhodamine B and 4-nitrophenol solutions with a stable poly-hydroxyl-iron/sepiolite catalyst. *Chem. Eng. J.* **2013**, *217*, 221−230.
(56) Caplow, M. Kinetics of carbamate formation and breakdown. *J. Am. Chem. Soc.* **1968**, *90*, 6795−6803.
(57) Hu, X. E.; Yu, Q.; Barzagli, F.; Li, C.; Fan, M.; Gasem, K. A. M.; Zhang, X.; Shiko, E.; Tian, M.; Luo, X.; Zeng, Z.; Liu, Y.; Zhang, R. NMR techniques and prediction models for the analysis of species formed in CO_2 capture processes with amine-based sorbents: A critical review. *ACS Sustain. Chem. Eng.* **2020**, *8*, 6173−6193.
(58) Chen, G.; Chen, G.; Peruzzini, M.; Zhang, R.; Barzagli, F. Understanding the potential benefits of blended ternary amine systems for CO_2 capture processes through ^{13}C NMR speciation study and energy cost analysis. *Sep. Purif. Technol.* **2022**, *291*, No. 120939.
(59) Zhang, R.; Liang, Z.; Liu, H.; Rongwong, W.; Luo, X.; Idem, R.; Yang, Q. Study of formation of bicarbonate ions in CO_2-loaded aqueous single 1DMA2P and MDEA tertiary amines and blended MEA−1DMA2P and MEA−MDEA amines for low heat of regeneration. *Ind. Eng. Chem. Res.* **2016**, *55*, 3710−3717.

https://doi.org/10.1021/acssuschemeng.2c06739
ACS Sustainable Chem. Eng. XXXX, XXX, XXX−XXX